Numerical study of stream-function formulation governing flows in multiply-connected domains by integrated RBFs and Cartesian grids

K. Le-Cao[1], N. Mai-Duy[1,*], C.-D. Tran[1,2] and T. Tran-Cong[1]

[1] Computational Engineering and Science Research Centre

Faculty of Engineering and Surveying,

The University of Southern Queensland, Toowoomba, QLD 4350, Australia

[2] CSIRO, Geelong,VIC 3216, Australia

Submitted to *Computers & Fluids*, 31-March-2010; revised, 3-September-2010

*Corresponding author: E-mail nam.mai-duy@usq.edu.au, Telephone +61 7 4631 2748, Fax +61 7 4631 2526

Abstract This paper describes a new numerical procedure, based on point collocation, integrated multiquadric functions and Cartesian grids, for the discretisation of the stream-function formulation for flows of a Newtonian fluid in multiply-connected domains. Three particular issues, namely (i) the derivation of the stream-function values on separate boundaries, (ii) the implementation of cross derivatives in irregular regions, and (iii) the treatment of double boundary conditions, are studied in the context of Cartesian grids and approximants based on integrated multiquadric functions in one dimension. Several test problems, i.e. steady flows between a rotating circular cylinder and a fixed square cylinder and also between eccentric cylinders maintained at different temperatures, are investigated. Results obtained are compared well with numerical data available in the literature.

Keywords: Stream-function formulation; multiply-connected domain; integrated radial basis function network; Cartesian grid

1 Introduction

The motion of a Newtonian fluid is governed by the Navier-Stokes equations which can be written in terms of different dependent variables, including the velocity - pressure formulation, the stream-function - vorticity formulation and the stream-function formulation. The velocity - pressure formulation is able to work for two- and three-dimension flows in a similar manner. One main concern is that there are no explicit transport equation and boundary conditions for the pressure variable. The resultant algebraic system could be solved iteratively where the pressure value is corrected using the continuity equation. For two-dimensional (2D) problems, by introducing the stream-function variable, one can eliminate the pressure and reduce the number of unknowns, i.e. from three (the velocity - pressure formulation) to

two (stream-function and vorticity) and only one (stream-function). However, the last two formulations have some drawbacks. Special attention should be given to the handling of the vorticity boundary condition for the stream-function - vorticity formulation and the double boundary conditions as well as high-order derivatives including the cross ones for the stream-function formulation. Furthermore, the pressure field needs be computed after solving the governing equations, which is generally regarded as a complicated process. In the case of multiply-connected domains, an added difficulty is that the stream-function variable generally has different values, which are unknown, on separate boundaries. It is noted that advantages of the stream-function - vorticity formulation presented above are restricted to 2D problems.

The governing differential equations can be transformed into sets of algebraic equations by means of discretisation. To support the approximations, the problem domain needs be represented by a set of finite elements, a Cartesian grid or a collection of discrete points. For problems with complicated geometries such as flows in multiply-connected domains, it has been recognised that the task of dividing the spatial domain into a number of finite elements can be the most time-consuming part of the solution process. Generating a Cartesian grid or a set of discrete points is clearly much more economical. Over the last twenty years, radial-basis-function networks (RBFNs) have been developed to solve different types of differential problems encountered in applied mathematics, science and engineering (e.g. [1,2,3,4,5,6,7,8,9]). These approximators can work well with gridded and scattered points. As shown in [10, 11, 12], there is the relation between the RBF collocation method and the finite difference method (FDM). For 1D approximations, the standard RBF interpolant converges to the Lagrange interpolating polynomial as the RBF width goes to infinity, which means that all classical FD formulas can be recovered by the limiting RBF interpolant. In the case of two and higher dimensions, the situation is not

clear due to the fact that multivariate polynomial interpolations are not well-posed.

In [4,5,6,7,8], the RBF approximations are constructed using integration (integrated RBFNs (IRBFNs)) rather than the usual differentiation. This approach has the ability to overcome the problem of reduced convergence rates caused by differentiation and to provide effective ways to implement derivative boundary values. IRBFNs have been developed for the simulation of flows in simply-connected domains governed by the stream-function formulation and the stream-function - vorticity formulation (e.g. [6]) as well as natural convection in regions between concentric cylinders governed by the stream-function - vorticity formulation (symmetrical flows) (e.g. [4]).

This study is concerned with the simulation of unsymmetrical flows of a Newtonian fluid in multiply-connected domains using the stream-function formulation, Cartesian grids and 1D-IRBFNs. Unlike the symmetrical case, the stream-function variable has different values on separate boundaries. These values can be found using the single-value condition for the pressure, whose implementations are known to be difficult (e.g. [13]). Further difficulties include the implementation of cross derivatives in regions bounded by irregular surfaces as the boundary points do not generally coincide with the grid nodes. New treatments for these difficulties and their 1D-IRBF-based implementations are the focal point of this study.

An outline of the paper is as follows. The stream-function formulation and 1D-IRBFNs are briefly reviewed in Section 2 and Section 3, respectively. The proposed procedure is described in Section 4 and then numerically verified through the simulation of steady flows between a rotating circular cylinder and a fixed square cylinder and also between eccentric cylinders maintained at different temperatures in Section 5. Section 6 concludes the paper.

2 Governing equations

Consider the stream-function formulation. The non-dimensional basic equations for natural convection under the Boussinesq approximation in the Cartesian $x-y$ coordinate system can be written as (e.g. [14])

$$\frac{\partial}{\partial t}\left(\frac{\partial^2\psi}{\partial x^2}+\frac{\partial^2\psi}{\partial y^2}\right)+\frac{\partial\psi}{\partial y}\left(\frac{\partial^3\psi}{\partial x^3}+\frac{\partial^3\psi}{\partial x\partial y^2}\right)-\frac{\partial\psi}{\partial x}\left(\frac{\partial^3\psi}{\partial x^2\partial y}+\frac{\partial^3\psi}{\partial y^3}\right)$$
$$=\sqrt{\frac{Pr}{Ra}}\left(\frac{\partial^4\psi}{\partial x^4}+2\frac{\partial^4\psi}{\partial x^2\partial y^2}+\frac{\partial^4\psi}{\partial y^4}\right)-\frac{\partial T}{\partial x}, \tag{1}$$

$$\frac{\partial T}{\partial t}+u\frac{\partial T}{\partial x}+v\frac{\partial T}{\partial y}=\frac{1}{\sqrt{RaPr}}\left(\frac{\partial^2 T}{\partial x^2}+\frac{\partial^2 T}{\partial y^2}\right), \tag{2}$$

where ψ is the stream function, T the temperature, t the time, u and v the velocity components, and Pr and Ra the Prandtl and Rayleigh numbers defined as $Pr=\nu/\alpha$ and $Ra=\beta g\Delta T L^3/\alpha\nu$, respectively, in which ν is the kinematic viscosity, α the thermal diffusivity, β the thermal expansion coefficient and g the gravity. In this dimensionless scheme, L, ΔT (temperature difference), $U=\sqrt{gL\beta\Delta T}$ and (L/U), are taken as scale factors for length, temperature, velocity and time, respectively. It is noted that the velocity scale is chosen here in a way in which the buoyancy and inertial forces are balanced (e.g. [14]).

For iso-thermal flows, the non-dimensional basic equations reduce to

$$\frac{\partial}{\partial t}\left(\frac{\partial^2\psi}{\partial x^2}+\frac{\partial^2\psi}{\partial y^2}\right)+\frac{\partial\psi}{\partial y}\left(\frac{\partial^3\psi}{\partial x^3}+\frac{\partial^3\psi}{\partial x\partial y^2}\right)-\frac{\partial\psi}{\partial x}\left(\frac{\partial^3\psi}{\partial x^2\partial y}+\frac{\partial^3\psi}{\partial y^3}\right)=$$
$$\frac{1}{Re}\left(\frac{\partial^4\psi}{\partial x^4}+2\frac{\partial^4\psi}{\partial x^2\partial y^2}+\frac{\partial^4\psi}{\partial y^4}\right), \tag{3}$$

where Re is the Reynolds number defined as $Re=UL/\nu$.

The velocity components are defined in terms of the stream function as

$$u = \frac{\partial \psi}{\partial y}, \tag{4}$$

$$v = -\frac{\partial \psi}{\partial x}. \tag{5}$$

The given velocity boundary conditions for u and v can be transformed into two boundary conditions on the stream function and its normal derivative

$$\psi = \gamma, \tag{6}$$

$$\frac{\partial \psi}{\partial n} = \xi, \tag{7}$$

where n is the direction normal to the boundary, and γ and ξ prescribed functions. For the case of fixed concentric cylinders, non-slip boundary conditions usually lead to $\gamma = 0$ and $\xi = 0$ at walls. For the case of rotating cylinders and eccentric cylinders, because of the existence of a global circulation flow, the stream-function values on the inner and outer cylinder walls cannot be the same.

3 Brief review of 1D-integrated RBFNs

In contrast to the traditional/direct/differential approach, where a function f is approximated by an RBFN, followed by successive differentiations to obtain approximate expressions for its derivatives, the indirect/integral approach uses integration to construct the RBF approximations (e.g. [7,8]). A highest-order derivative of f under consideration, e.g. $d^p f(x)/dx^p$, is decomposed into RBFs, and lower-order

derivatives and the function itself are then obtained through integration

$$\frac{d^p f(x)}{dx^p} = \sum_{i=1}^{m} w_i g_i(x) = \sum_{i=1}^{m} w_i I_i^{(p)}(x), \tag{8}$$

$$\frac{d^{p-1} f(x)}{dx^{p-1}} = \sum_{i=1}^{m} w_i I_i^{(p-1)}(x) + c_1, \tag{9}$$

$$\frac{d^{p-2} f(x)}{dx^{p-2}} = \sum_{i=1}^{m} w_i I_i^{(p-2)}(x) + c_1 x + c_2, \tag{10}$$

$$\cdots \quad \cdots \quad \cdots \quad \cdots \quad \cdots$$

$$\frac{df(x)}{dx} = \sum_{i=1}^{m} w_i I_i^{(1)}(x) + c_1 \frac{x^{p-2}}{(p-2)!} + c_2 \frac{x^{p-3}}{(p-3)!} + \cdots + c_{p-2} x + c_{p-1}, \tag{11}$$

$$f(x) = \sum_{i=1}^{m} w_i I_i^{(0)}(x) + c_1 \frac{x^{p-1}}{(p-1)!} + c_2 \frac{x^{p-2}}{(p-2)!} + \cdots + c_{p-1} x + c_p, \tag{12}$$

where $\{g_i(x)\}_{i=1}^m \equiv \left\{I_i^{(p)}(x)\right\}_{i=1}^m$ is the set of RBFs, m the number of RBFs, $(c_1, c_2, \cdots, c_p)$ the constants of integration and $I_i^{(p-1)}(x) = \int I_i^{(p)}(x)dx$, $I_i^{(p-2)}(x) = \int I_i^{(p-1)}(x)dx, \cdots, I_i^{(0)}(x) = \int I_i^{(1)}(x)dx$. Numerical results (e.g. [7]) have shown that the integral approach significantly improves the quality of the approximation of derivative functions over conventional differential approaches. The IRBF-based approximation scheme is said to be of pth-order, denoted by IRBFN-p, if the pth-order derivative is taken as the staring point.

The present technique implements the multiquadric (MQ) function whose form is

$$g_i(x) = \sqrt{(x - c_i)^2 + a_i^2}, \tag{13}$$

where c_i and a_i are, respectively, the centre and the width of the ith MQ basis function.

4 Proposed numerical procedure

Calculations for unsymmetrical flows in multiply-connected domains are carried out on Cartesian grids. Grid nodes inside the domain of interest are taken to be interior nodes. Boundary points are generated by the intersection of the grid lines and boundaries. Boundary nodes are thus comprised of two sets of points. The first set is generated by the $x-$grid lines; the other by the $y-$grid lines.

1D-IRBFNs of orders 4 and 2 are employed on the grid lines to represent the stream-function and temperature variables, respectively. The governing differential equations, which involve high-order and cross derivatives, are discretised by means of point collocation. Emphasis is placed on the following issues: (i) the implementation of cross derivatives in irregular regions, (ii) the derivation of the stream-function values on separate boundaries, and (iii) the treatment of double boundary conditions. Formulas are derived in terms of Cartesian coordinates and they are implemented with 1D-IRBFNs.

It is noted that conventional RBF methods are global and lead to full matrices. Unlike conventional methods, at a grid node, the proposed method only uses RBF centres on the two associated grid lines rather than the whole set of RBF centres to construct the approximations at that point. The present method thus possesses some local approximation properties. In comparison with conventional RBF methods, relatively-large numbers of nodes can be employed here. However, the resultant system matrix is still not as sparse as those produced by finite-difference methods. The present technique needs be combined with domain decompositions for handling large-scale engineering problems.

4.1 Boundary values for stream function

Since there is no flow in the direction normal to a solid boundary, the stream function is constant at a wall. The stream-function variable has different values on different walls. The value of ψ on the outer wall is simply set to zero, while the values of ψ on inner walls are considered as unknowns. Consider an inner wall. The associated unknown there cannot be determined from the governing equation; an independent equation/integral condition is needed. To find the value of ψ on the wall, Lewis [15] suggested using the condition that the pressure is a single-valued function (there is only one value of pressure at a point). This condition can be mathematically described as

$$\oint_{\Gamma} \frac{\partial p}{\partial s} ds = \oint_{\Gamma} \nabla p \cdot d\vec{s} = 0, \tag{14}$$

where p is the pressure, s the arc length, ds the length of an infinitesimal part of the boundary Γ. It should be pointed out that Γ can be any closed path. In the present work, the inner cylinder boundary is taken to be Γ . The pressure gradient ∇p can be obtained from the momentum equations. The reader is referred to, for example, ([15, 16, 17]) for further details. In the Cartesian coordinate system, Equation (14) becomes

$$\oint \frac{\partial p}{\partial x} dx + \oint \frac{\partial p}{\partial y} dy = 0. \tag{15}$$

From the primitive variable formulation, we have

$$\frac{\partial p}{\partial x} = \frac{1}{Re}\left(\frac{\partial^2 u}{\partial x^2} + \frac{\partial^2 u}{\partial y^2}\right) - \left(u\frac{\partial u}{\partial x} + v\frac{\partial u}{\partial y}\right), \tag{16}$$

$$\frac{\partial p}{\partial y} = \frac{1}{Re}\left(\frac{\partial^2 v}{\partial x^2} + \frac{\partial^2 v}{\partial y^2}\right) - \left(u\frac{\partial v}{\partial x} + v\frac{\partial v}{\partial y}\right). \tag{17}$$

Substituting (16) and (17) into (15) and then making use of (4) and (5) lead to

$$\oint \frac{\partial^3 \psi}{\partial^2 x \partial y} dx + \oint \frac{\partial^3 \psi}{\partial^3 y} dx - Re \oint \frac{\partial \psi}{\partial y} \frac{\partial^2 \psi}{\partial x \partial y} dx + Re \oint \frac{\partial \psi}{\partial x} \frac{\partial^2 \psi}{\partial y^2} dx -$$
$$\oint \frac{\partial^3 \psi}{\partial^3 x} dy - \oint \frac{\partial^3 \psi}{\partial^2 y \partial x} dy + Re \oint \frac{\partial \psi}{\partial y} \frac{\partial^2 \psi}{\partial x^2} dy - Re \oint \frac{\partial \psi}{\partial x} \frac{\partial^2 \psi}{\partial y \partial x} dy = 0. \tag{18}$$

In the case of a fixed cylinder, the convection term vanishes on its wall. Equation (18) thus reduces to

$$\oint \frac{\partial^3 \psi}{\partial^2 x \partial y} dx + \oint \frac{\partial^3 \psi}{\partial^3 y} dx - \oint \frac{\partial^3 \psi}{\partial^3 x} dy - \oint \frac{\partial^3 \psi}{\partial^2 y \partial x} dy = 0. \tag{19}$$

By expressing integrals in (18)/(19) in terms of the values of ψ at the interior points, the resultant equation can be used as an extra equation to determine the value of ψ on the wall.

4.2 Cross derivatives

In the present formulations, the governing equations and the single-valued pressure condition involve cross derivatives, namely $\partial^4 \psi / \partial^2 x \partial^2 y$, $\partial^3 \psi / \partial^2 x \partial y$, and $\partial^3 \psi / \partial x \partial y^2$. As mentioned earlier, the IRBF approximations are constructed on the grid lines. It is necessary to transform the computation of these mixed derivatives to that of pure derivatives. This can be achieved through the following relations

$$\frac{\partial^4 \psi}{\partial^2 x \partial^2 y} = \frac{1}{2} \left[\frac{\partial^2}{\partial x^2} \left(\frac{\partial^2 \psi}{\partial y^2} \right) + \frac{\partial^2}{\partial y^2} \left(\frac{\partial^2 \psi}{\partial x^2} \right) \right], \tag{20}$$

$$\frac{\partial^3 \psi}{\partial^2 x \partial y} = \frac{\partial^2}{\partial x^2} \left(\frac{\partial \psi}{\partial y} \right), \tag{21}$$

$$\frac{\partial^3 \psi}{\partial x \partial y^2} = \frac{\partial^2}{\partial y^2} \left(\frac{\partial \psi}{\partial x} \right). \tag{22}$$

In (20)-(22), there are two terms, namely $\partial^2\left(\partial^2\psi/\partial y^2\right)/\partial x^2$ and $\partial^2\left(\partial\psi/\partial y\right)/\partial x^2$, to be evaluated on the $x-$grid lines and two terms, namely $\partial^2\left(\partial^2\psi/\partial x^2\right)/\partial y^2$ and $\partial^2\left(\partial\psi/\partial x\right)/\partial y^2$, to be evaluated on the $y-$grid lines.

Consider an $x-$grid line. To carry out the approximation of $\partial^2\left(\partial^2\psi/\partial y^2\right)/\partial x^2$ and $\partial^2\left(\partial\psi/\partial y\right)/\partial x^2$, the values of $\partial^2\psi/\partial y^2$ and $\partial\psi/\partial y$ at the interior and boundary nodes on the $x-$grid line are assumed to be given (i.e. they are known values or can be expressed in terms of the nodal values of ψ). For nodal interior points, these values can be obtained straightforwardly by using the approximations on the vertical grid lines. For the boundary points, the value of $\partial\psi/\partial y$ is known as it can be easily computed from the given boundary conditions ψ and $\partial\psi/\partial n$, while one does not generally know the value of $\partial^2\psi/\partial y^2$. For the latter, there are two possible cases. If the boundary point is also a grid node, the computation of $\partial^2\psi/\partial y^2$ is similar to that of an interior point. If the boundary point is not a grid node, special treatment is required. A new formula for computing $\partial^2\psi/\partial y^2$ is derived as follows. Along a curved boundary (Figure 1), the values of $\partial\psi/\partial x$ and $\partial\psi/\partial y$ can be easily obtained from the prescribed boundary values for ψ and $\partial\psi/\partial n$. By introducing an interpolating scheme (e.g. 1D-IRBFNs) on the boundary, one is able to get derivatives of $\partial\psi/\partial x$ and $\partial\psi/\partial y$ along the boundary such as $\partial^2\psi/\partial x\partial s$ and $\partial^2\psi/\partial y\partial s$ in which s is the arc-length of the curved boundary. A tangential derivative of a generic function f at a boundary point, x_b, can be computed by

$$\frac{\partial f}{\partial s} = \frac{\partial f}{\partial x}t_x + \frac{\partial f}{\partial y}t_y, \tag{23}$$

where $t_x = \partial x/\partial s$ and $t_y = \partial y/\partial s$ are the two x and y components of the unit vector tangent to the curve.

Replacing f with $\partial\psi(x_b)/\partial x$, we have

$$\frac{\partial^2\psi(x_b)}{\partial x\partial s} = \frac{\partial^2\psi(x_b)}{\partial x^2}t_x + \frac{\partial^2\psi(x_b)}{\partial x\partial y}t_y, \tag{24}$$

or

$$\frac{\partial^2\psi(x_b)}{\partial x\partial y} = \frac{1}{t_y}\left(\frac{\partial^2\psi(x_b)}{\partial x\partial s} - \frac{\partial^2\psi(x_b)}{\partial x^2}t_x\right), \tag{25}$$

where the value of $\partial^2\psi(x_b)/\partial x\partial s$ is known.

Similarly, taking f as $\partial\psi(x_b)/\partial y$ results in

$$\frac{\partial^2\psi(x_b)}{\partial x\partial y} = \frac{1}{t_x}\left(\frac{\partial^2\psi(x_b)}{\partial y\partial s} - \frac{\partial^2\psi(x_b)}{\partial y^2}t_y\right). \tag{26}$$

From (25) and (26), one can derive the relation between $\partial^2\psi/\partial x^2$ and $\partial^2\psi/\partial y^2$ at a boundary point

$$\frac{1}{t_y}\left(\frac{\partial^2\psi(x_b)}{\partial x\partial s} - \frac{\partial^2\psi(x_b)}{\partial x^2}t_x\right) = \frac{1}{t_x}\left(\frac{\partial^2\psi(x_b)}{\partial y\partial s} - \frac{\partial^2\psi(x_b)}{\partial y^2}t_y\right). \tag{27}$$

Expression (27) can be rearranged as

$$\frac{\partial^2\psi(x_b)}{\partial y^2} = \left(\frac{t_x}{t_y}\right)^2\frac{\partial^2\psi(x_b)}{\partial x^2} + q_y, \tag{28}$$

where q_y is a known value defined by

$$q_y = -\frac{t_x}{t_y^2}\frac{\partial^2\psi(x_b)}{\partial x\partial s} + \frac{1}{t_y}\frac{\partial^2\psi(x_b)}{\partial y\partial s}. \tag{29}$$

Formula (28) facilitates the computation of the value of $\partial^2\psi/\partial y^2$ at a boundary point x_b using the approximations on the $x-$grid line.

Consider an $y-$grid line. In the same manner, the value of $\partial^2\psi/\partial x^2$ at a boundary

point y_b can be computed by

$$\frac{\partial^2 \psi(y_b)}{\partial x^2} = \left(\frac{t_y}{t_x}\right)^2 \frac{\partial^2 \psi(y_b)}{\partial y^2} + q_x, \tag{30}$$

where q_x is a known value defined by

$$q_x = -\frac{t_y}{t_x^2}\frac{\partial^2 \psi(y_b)}{\partial y \partial s} + \frac{1}{t_x}\frac{\partial^2 \psi(y_b)}{\partial x \partial s}. \tag{31}$$

It can be seen that, given a Cartesian grid, expressions (28) and (30) allow the approximations of mixed derivatives in regions bounded by irregular surfaces to be expressed in terms of the nodal values of ψ and the boundary conditions.

4.3 1D-IRBF expressions

1D-IRBF expressions on the $x-$ and $y-$grid lines have similar forms. In the following, the process of deriving 1D-IRBF expressions for the stream-function variable and its derivatives on the $x-$grid lines is presented in detail.

4.3.1 Pure derivatives

Along an $x-$grid line (Figure 2), the set of RBF centres consists of the interior points $\{x_i\}_{i=1}^{q}$ and the two boundary points $\{x_{bi}\}_{i=1}^{2}$. The stream-function variable is approximated using 1D-IRBFN-4s. At a boundary point x_b, there are double boundary conditions, $\psi(x_b)$ and $\partial\psi(x_b)/\partial x$. Unlike conventional differentiated RBFNs, there are four integration constants in the 1D-IRBFN formulation. These extra coefficients allows for the addition of some extra equations to the process of conversion of the coefficient space into the physical space. The extra equations are utilised here

to implement derivative boundary values

$$\begin{pmatrix} \widehat{\psi} \\ \widehat{\psi_b} \\ \widehat{\frac{\partial \psi_b}{\partial x}} \end{pmatrix} = \widehat{\mathcal{C}}\, \widehat{w}, \tag{32}$$

where

$$\begin{aligned}
\widehat{\psi} &= (\psi(x_1), \psi(x_2), \cdots, \psi(x_q))^T, \\
\widehat{\psi_b} &= (\psi(x_{b1}), \psi(x_{b2}))^T, \\
\widehat{\frac{\partial \psi_b}{\partial x}} &= \left(\frac{\partial \psi(x_{b1})}{\partial x}, \frac{\partial \psi(x_{b2})}{\partial x} \right)^T, \\
\widehat{\mathcal{C}} &= \begin{bmatrix}
I_1^{(0)}(x_1) & \cdots & I_m^{(0)}(x_1) & x_1^3/6 & x_1^2/2 & x_1 & 1 \\
I_1^{(0)}(x_2) & \cdots & I_m^{(0)}(x_2) & x_2^3/6 & x_2^2/2 & x_2 & 1 \\
\vdots & \ddots & \vdots & \vdots & \vdots & \vdots & \vdots \\
I_1^{(0)}(x_q) & \cdots & I_m^{(0)}(x_q) & x_q^3/6 & x_q^2/2 & x_q & 1 \\
I_1^{(0)}(x_{b1}) & \cdots & I_m^{(0)}(x_{b1}) & x_{b1}^3/6 & x_{b1}^2/2 & x_{b1} & 1 \\
I_1^{(0)}(x_{b2}) & \cdots & I_m^{(0)}(x_{b2}) & x_{b2}^3/6 & x_{b2}^2/2 & x_{b2} & 1 \\
I_1^{(1)}(x_{b1}) & \cdots & I_m^{(1)}(x_{b1}) & x_{b1}^2/2 & x_{b1} & 1 & 0 \\
I_1^{(1)}(x_{b2}) & \cdots & I_m^{(1)}(x_{b2}) & x_{b2}^2/2 & x_{b2} & 1 & 0
\end{bmatrix}, \\
\widehat{w} &= (w_1, w_2, \cdots, w_m, c_1, c_2, c_3, c_4)^T,
\end{aligned}$$

and $m = q + 2$. The values of the lth-order derivative ($l = \{1, 2, 3, 4\}$) of ψ at the interior points on the grid line are evaluated as

$$\widehat{\frac{\partial^l \psi}{\partial x^l}} = \widehat{\mathcal{I}}_{[4]}^{(l)} \widehat{\mathcal{C}}^{-1} \begin{pmatrix} \widehat{\psi} \\ \widehat{\psi_b} \\ \widehat{\frac{\partial \psi_b}{\partial x}} \end{pmatrix}, \tag{33}$$

where

$$\widehat{\mathcal{I}}^{(4)}_{[4]} = \begin{bmatrix} I^{(4)}_1(x_1) & \cdots & I^{(4)}_m(x_1) & 0 & 0 & 0 & 0 \\ I^{(4)}_1(x_2) & \cdots & I^{(4)}_m(x_2) & 0 & 0 & 0 & 0 \\ \vdots & \ddots & \vdots & \vdots & \vdots & \vdots & \vdots \\ I^{(4)}_1(x_q) & \cdots & I^{(4)}_m(x_q) & 0 & 0 & 0 & 0 \end{bmatrix},$$

$$\widehat{\mathcal{I}}^{(3)}_{[4]} = \begin{bmatrix} I^{(3)}_1(x_1) & \cdots & I^{(3)}_m(x_1) & 1 & 0 & 0 & 0 \\ I^{(3)}_1(x_2) & \cdots & I^{(3)}_m(x_2) & 1 & 0 & 0 & 0 \\ \vdots & \ddots & \vdots & \vdots & \vdots & \vdots & \vdots \\ I^{(3)}_1(x_q) & \cdots & I^{(3)}_m(x_q) & 1 & 0 & 0 & 0 \end{bmatrix},$$

$$\widehat{\mathcal{I}}^{(2)}_{[4]} = \begin{bmatrix} I^{(2)}_1(x_1) & \cdots & I^{(2)}_m(x_1) & x_1 & 1 & 0 & 0 \\ I^{(2)}_1(x_2) & \cdots & I^{(2)}_m(x_2) & x_2 & 1 & 0 & 0 \\ \vdots & \ddots & \vdots & \vdots & \vdots & \vdots & \vdots \\ I^{(2)}_1(x_q) & \cdots & I^{(2)}_m(x_q) & x_q & 1 & 0 & 0 \end{bmatrix},$$

and

$$\widehat{\mathcal{I}}^{(1)}_{[4]} = \begin{bmatrix} I^{(1)}_1(x_1) & \cdots & I^{(1)}_m(x_1) & x_1^2/2 & x_1 & 1 & 0 \\ I^{(1)}_1(x_2) & \cdots & I^{(1)}_m(x_2) & x_2^2/2 & x_2 & 1 & 0 \\ \vdots & \ddots & \vdots & \vdots & \vdots & \vdots & \vdots \\ I^{(1)}_1(x_q) & \cdots & I^{(1)}_m(x_q) & x_q^2/2 & x_q & 1 & 0 \end{bmatrix}.$$

Expressions (33) can be rewritten in compact form

$$\widehat{\frac{\partial^l \psi}{\partial x^l}} = \widehat{\mathcal{D}}_{lx}\widehat{\psi} + \widehat{k}_{lx}, \tag{34}$$

where $\widehat{\mathcal{D}}_{lx}$ are the differentiation matrices in the physical space, and $\widehat{k}_{lx}$ the vectors whose components are functions of boundary conditions. It is noted that, for the grid lines which cross over the inner cylinder, only the values of ψ on the outer cylinder are given.

Similarly, 1D-IRBFN expressions for pure derivatives on the $y-$grid lines take the following forms

$$\widehat{\frac{\partial^l \psi}{\partial y^l}} = \widehat{\mathcal{D}}_{ly}\widehat{\psi} + \widehat{k}_{ly}, \tag{35}$$

where $l = \{1, 2, 3, 4\}$.

4.3.2 Mixed derivatives

On an $x-$grid line, it can be seen from (20)-(22) that relevant mixed derivative to be evaluated here are $\partial^2 \left(\partial\psi/\partial y\right)/\partial x^2$ and $\partial^2 \left(\partial^2\psi/\partial y^2\right)/\partial x^2$. Approximate expressions for $\partial\psi/\partial y$ and $\partial^2\psi/\partial y^2$ can be obtained at the interior points using (35) with $l = \{1, 2\}$. At the boundary points, the values of $\partial\psi/\partial y$ are given, while the values of $\partial^2\psi/\partial y^2$ can be computed using (28) in which $\partial^2\psi/\partial x^2$ is evaluated using the nodal values of ψ on the $x-$grid line

$$\frac{\partial^2\psi(x_b)}{\partial x^2} = \left[\begin{array}{ccccccc} I_1^{(2)}(x_b) & \cdots & I_m^{(2)}(x_b) & x_b & 1 & 0 & 0 \end{array}\right] \widehat{\mathcal{C}}^{-1} \left(\begin{array}{c} \widehat{\psi} \\ \widehat{\psi}_b \\ \widehat{\frac{\partial\psi_b}{\partial x}} \end{array}\right), \tag{36}$$

where x_b is a boundary point and $\widehat{\psi}, \widehat{\partial\psi}_b/\partial x, \widehat{w}$ and $\widehat{\mathcal{C}}$ are defined as before.

Let g represent $\partial^2\psi/\partial y^2$ and $\partial\psi/\partial y$. The remaining task is to form an 1D-IRBF expression for $\partial^2 g/\partial x^2$. This process is similar to that for the stream function which is described in Section 4.3.1, except that there are no extra equations representing derivative boundary values in (32).

4.3.3 Single-valued pressure equation

As shown in (18)/(19), this pressure condition involves pure and mixed derivatives on the wall.

Using 1D-IRBFN expressions which are derived above, one can express derivatives in (18)/(19) in terms of the nodal values of ψ. For example, the integrand of the third term in (19) can be written as

$$\frac{\partial^3 \psi(x_b)}{\partial x^3} = \left[\begin{array}{ccccc} I_1^{(3)}(x_b) \cdots I_m^{(3)}(x_b) & 1 & 0 & 0 & 0 \end{array} \right] \widehat{\mathcal{C}}^{-1} \left(\begin{array}{c} \widehat{\psi} \\ \widehat{\psi}_b \\ \widehat{\frac{\partial \psi_b}{\partial x}} \end{array} \right), \tag{37}$$

where x_b is the boundary point on the inner wall and $\widehat{\psi}, \widehat{\partial \psi}_b/\partial x, \widehat{w}$ and $\widehat{\mathcal{C}}$ are defined as before. The vector $\widehat{\psi}_b$ in (37) contains the value of the stream function on the inner cylinder, i.e. $\psi(x_b)$, that is an unknown to be found.

All associated integrals in (18)/(19) are then evaluated using the Gauss quadrature scheme.

The pressure condition leads to a relation where the value of ψ on the inner wall is expressed as a linear combination of the values of ψ at the interior points.

4.4 Solution Procedure

The algebraic equation set resulting from the discretisation of the stream-function formulation is nonlinear because of the presence of the convective terms. There are two approaches widely used to handle this nonlinearity. In the first approach, all time derivative terms are dropped out and nonlinear solvers such as Newton iterations

can be applied. In the second approach, the solution is obtained by means of time marching. Each approach has some advantages over the other for certain problems. In this study, fluid flow problems are considered and the second approach is applied.

1. Guess initial values of T, ψ and their spatial derivatives at time $t = 0$.

2. Discretise the governing equations in time using a first-order accurate finite-difference scheme, where the diffusive and convective terms are treated implicitly and explicitly, respectively.

3. Discretise the governing equations in space using 1D-IRBF schemes,
   Solve the energy equation (2) for T, and
   Solve the momentum equation (1) for ψ.
   The two equations are solved separately in order to keep matrix sizes to a minimum.

4. Check to see whether the solution has reached a steady state

$$CM = \frac{\sqrt{\sum_{i=1}^{n_{ip}} \left(\psi_i^{(k)} - \psi_i^{(k-1)}\right)^2}}{\sqrt{\sum_{i=1}^{n_{ip}} \left(\psi_i^{(k)}\right)^2}} < \epsilon, \tag{38}$$

   where k is the time level and ϵ is the prescribed tolerance.

5. If it is not satisfied, advance time step and repeat from step 2. Otherwise, stop the computation and output the results.

5 Numerical results

The present method is verified through the simulation of steady iso-thermal flows between a rotating circular cylinder and a fixed square cylinder, and steady buoyancy-

driven flows in eccentric annuli with a wide range of the eccentricity. The computed solution at the lower and nearest value of Re/Ra is taken to be the initial solution. Internal grid points that fall very close–within a distance of $h/8$–to the boundary are removed.

It is well known that RBF-based schemes suffer from the so-called uncertainty or trade-off principle. As the value of the RBF-width/shape-parameter increases, the approximation error reduces while the condition number of the system matrix grows. Unfortunately, there is still a lack of theory to determine the optimal value for the RBF width. The RBF width is usually chosen by trial and error or some other ad-hoc means. In this study, the grid size h is taken to be the MQ-RBF width.

For conventional FDMs and pseudo-spectral techniques, coordinate transformations are required to convert non-rectangular domains into rectangular ones [16,18]. The relationships between the physical and computational coordinates are given by a set of algebraic equations or a set of partial differential equations (PDEs), depending on the level of complexity of the geometry. Such transformation processes are, in general, complicated. The proposed technique can work with irregular domains in a direct manner, i.e. without the need for using coordinate transformations. However, the proposed technique is restricted to structured uniform or non-uniform Cartesian grids.

5.1 Example 1: Steady flow between a rotating circular cylinder and a fixed square cylinder

This test problem is employed for the investigation of accuracy of the proposed technique in computing the value of the stream function on the inner cylinder. The flow geometry and discretisation are shown in Figure 3. The inner cylinder rotates

at a unit angular velocity. The stream function on the outer wall is set to zero. Formula (18) is utilised to determine the value of the stream function on the inner wall, denoted by ψ_w. This flow is governed by (3) and subject to the boundary conditions

$$\psi = \frac{\partial \psi}{\partial x} = \frac{\partial \psi}{\partial y} = 0,$$

on the outer cylinder and

$$\psi = \psi_w, \quad \frac{\partial \psi}{\partial x} = -x, \quad \frac{\partial \psi}{\partial y} = -y,$$

on the inner cylinder. The flow is simulated with $R = 0.25$ and $L = \{0.55, 1.0\}$ using a uniform grid of 52×52. Different values of the Reynolds number, namely 1, 100, 500, 700 and 1000, are considered. Results concerning ψ_w obtained by the proposed technique and the finite-difference technique [15] are presented in Table 1, showing a satisfactory agreement. Plots for the velocity and vorticity fields for the case of $L = 1$ and $R = 0.5$ at $Re = \{1, 700\}$ are given in Figure 4.

5.2 Example 2: Natural convection in an eccentric annulus between two circular cylinders

Natural convection is governed by the coupling of the momentum equation (velocity field) (1) and energy equation (temperature field) (2). Solutions to natural convection in concentric and eccentric annuli between two circular cylinders have been reported using various discretisation techniques such as finite-difference methods (FDMs) (e.g. [19,20]), finite-element methods (FEMs) (e.g. [21,22]), finite-volume methods (FVMs) (e.g. [23,24]), boundary-element methods (BEMs) (e.g. [25,26]) and spectral methods (e.g. [16,17,27,28]).

Consider buoyancy-driven flows of a Newtonian fluid between two cylinders whose centres are separated by a distance ε (Figure 5). As shown in Figure 5, the flow geometry is defined by the following geometrical parameters: the eccentricity ε, angular position φ, the diameter of the outer cylinder D_o and the diameter of the inner cylinder D_i. In the present work, the numerical results are reported with $Pr = 0.71$ and $D_o/D_i = 2.6$. A typical discretisation is shown on Figure 6a, where no coordinate transformations are employed.

The inner and outer cylinders are heated ($T = 1$) and cooled ($T = 0$), respectively. The stream-function value at the outer cylinder is set to zero. The stream-function value at the inner cylinder is a part of the solution and can be determined by the single-valued pressure condition (19). The normal derivatives of the stream function are set to zero at both walls.

One typical quantity associated with this type of flow is the average equivalent conductivity denoted by $\bar{k}_{eq}$. This quantity is defined as (e.g. [20])

$$\bar{k}_{eq} = \frac{-\ln(D_o/D_i)}{2\pi} \oint \frac{\partial T}{\partial n} ds \tag{39}$$

The present method is first tested with the case of symmetrical flows. For such flows, one is able to know the exact solution of ψ at the inner wall ($\psi_w = 0$), which can be used to test numerical solvers. We employ three uniform grids of 41×41, 51×51 and 61×61 to represent the flow field. Results obtained show that the value of ψ_w is less than 10^{-6}. For concentric cylinders, results concerning $\bar{k}_{eq}$ by the present technique together with those by FDMs [20] and DQMs [16] for $Ra = 7 \times 10^4$ are presented in Table 2. The present solutions converge well and are in close agreement with the other solutions. It can be seen that the IRBF results are more agreeable to the DQ ones than the FD results. For eccentric cylinders (i.e. the centres of inner and outer cylinders lie on the vertical symmetrical axis), Table 3 compares

the maximum value of ψ for $Ra = 10^4$ between the proposed method and the DQM [16]. Good agreement is achieved.

For the case of unsymmetrical flows, the value of ψ at the inner wall has non-zero value that varies with the location of the inner cylinder. Different amounts of eccentricity (ε), namely $\{0.25, 0.5, 0.75, 0.95\}$, and angular direction φ, namely $\{-90^0, -45^0, 0^0, 45^0, 90^0\}$, are employed. In Table 4, the values of ψ at the inner walls are presented and agree satisfactorily with those conducted by the DQM [16] and the domain free discretisation method (DFD) [17]. Figure 7 shows the streamlines and isotherms of the flow at $Ra = 10^4$ using a grid of 61×61, where different values of eccentricity and angular directions are employed. Each plot contains 21 contour lines whose levels vary linearly from the minimum to maximum values. All plots look reasonable when compared with those of the DQM [16].

5.3 Example 3: Natural convection in an eccentric annulus between a square outer and a circular inner cylinder

In this example, natural convection between a heated inner circular cylinder and a cooled square enclosure (Figure 8) is considered. An aspect ratio of $L/2R = 0.26$ (L: the side length of the outer square and R: the radius of the inner circle), $Pr = 0.71$ and $Ra = 3 \times 10^5$ are used.

The problem domain is simply replaced with a Cartesian grid (Figure 6b), where no coordinate transformations are employed.

Similar to Example 2, the eccentricity values used are $\varepsilon = \{0.25, 0.5, 0.75, 0.95\}$ and the angular positions are $\varphi = \{-90^0, -45^0, 0^0, 45^0, 90^0\}$. The value of ψ along the inner is considered as an unknown and the values of ψ along the outer boundaries

can be taken to be zero. Calculations are conducted on a uniform Cartesian grid of 62×62. In Table 5, the maximum values of the stream function are presented and compared very well with those conducted by Ding [29].

For special cases of eccentric square-circular annuli, where the centre of the inner cylinder lies on the vertical symmetrical axis of an outer cylinder, the values of ψ_{max} are given in Table 6. It can be seen that the present results are in very good agreement with those of Ding [29].

Following the work of Moukalled and Acharya [18], the local heat transfer coefficient is defined as

$$\theta = -k\frac{\partial T}{\partial n}, \tag{40}$$

where k is the thermal conductivity. The average Nusselt number (the ratio of the temperature gradient at the wall to a reference temperature gradient) is computed by

$$Nu = \frac{\overline{\theta}}{k}, \tag{41}$$

where $\overline{\theta} = -\oint \frac{\partial T}{\partial n} ds$. Since the computational domain in [18] is taken as one-half of the physical domain, the values of Nu in the present work (Table 7) are divided by 2 for comparison purposes. The present results agree well with those in [18] and [29].

Figures 9 displays streamline and isotherm fields with different positions of the inner cylinder for $Ra = 3 \times 10^5$. The qualitative behaviours of these fields and those in [29] are similar. In Figure 10, the effects of time step on the convergence of the proposed technique are investigated for the case of $Ra = 1 \times 10^5$ using a grid of 53×53. It can be seen that the present technique can work with a wide range of the value of time step. As expected, the convergence is faster but less stable when the length of time step increases. In relation to CPU times, the present technique

consumes 0.013715 (s) per iteration for a grid of 33×33, 0.0599 for 49×49 and 0.0807 for 53×53 (Intel Core 2 6300-1.86 Ghz).

For all values of the Reynolds/Rayleigh number employed in these examples, it is observed that the solution evolves in a stable manner with relatively-large time steps. As a result, the use of special treatments for the convection term such as the upwind scheme is not necessary here.

6 Concluding Remarks

In this article, flows in multiply-connected domains are studied using the stream-function formulation, one-dimensional integrated RBF approximations and Cartesian grids. Formulas for handling mixed derivatives in irregular regions and boundary conditions for the stream-function variable are derived under the Cartesian framework, and they are implemented effectively with 1D-IRBFNs. Attractive features of the proposed technique include (i) simple preprocessing and (ii) the ability to retain the PDEs in their Cartesian forms, and thus to work in a similar fashion for different shapes of annuli. Various solutions are reported to demonstrate the capabilities of the proposed technique.

Acknowledgements

This research is supported by the Australian Research Council. K. Le-Cao wishes to thank the USQ, CESRC and CSIRO for a postgraduate scholarship. The authors would like to thank the referees for their helpful comments.

References

[1] Fasshauer GE. Solving partial differential equations by collocation with radial basis functions, Surface Fitting and Multiresolution Methods. Nashville:Vanderbilt University Press; 1997.

[2] Kansa EJ. Multiquadrics- A scattered data approximation scheme with applications to computational fluid-dynamics-II. Solutions to parabolic, hyperbolic and elliptic partial differential equations. Computers and Mathematics with Applications 1990;19(8/9):147-161.

[3] Kosec G, Sarler B. Solution of thermo-fluid problems by collocation with local pressure correction. International Journal of Numerical Methods for Heat & Fluid Flow 2008;18(7/8):868-882.

[4] Le-Cao K, Mai-Duy N, Tran-Cong T. An effective integrated-rbfn cartesian-grid discretization for the stream function-vorticity-temperature formulation in nonrectangular domains. Numerical Heat Transfer, Part B: Fundamentals 2009;55(6):480-502.

[5] Mai-Duy N, Le-Cao K, Tran-Cong T. A Cartesian grid technique based on one-dimensional integrated radial basis function networks for natural convection in conccentric annuli. International Journal for Numerical Methods in Fluids 2008;57:1709-1730.

[6] Mai-Duy N, Tran-Cong T. Numerical solution of Navier-Stokes equations using multiquadric radial basis function networks. International Journal for Numerical Methods in Fluids 2001;37(1):65-86.

[7] Mai-Duy N, Tran-Cong T. Approximation of function and its derivatives using radial basis function networks. Applied Mathematical Modelling 2003;27:197-220.

[8] Mai-Duy N, Tran-Cong T. A Cartesian-grid collocation method based on radial-basis-function networks for solving PDEs in irregular domains. Numerical Methods for Partial Differential Equations 2007;23(5):1192-1210.

[9] Sarler B. A radial basis function collocation approach in computational fluid dynamics. Computer Modeling in Engineering and Sciences 2005;7(2):185-194.

[10] Driscoll TA, Fornberg B. Interpolation in the limit of increasingly flat radial basis functions. Computers and Mathematics with Applications 2002;43:413-422.

[11] Schaback R. Multivariate interpolation by polynomials and radial basis functions. Constructive Approximation 2005;21:293-317.

[12] Wright GB, Fornberg B. Scattered node compact finite difference-type formulas generated from radial basis functions. Journal of Computational Physics 2006; 212:99-123.

[13] Roger P. Spectral Methods for Incompressible Viscous Flow Series: Applied Mathematical Sciences, Vol. 148. New York: Springer-Verlag; 2002.

[14] Ostrach S. Natural convection in enclosures. Journal of Heat Transfer 1988;110:1175-1190.

[15] Lewis E. Steady flow between a rotating circular cylinder and fixed square cylinder. Journal of Fluid Mechanics. 1979;95:497-513.

[16] Shu C, Yao Q, Yeo KS, Zhu YD. Numerical analysis of flow and thermal fields in arbitrary eccentric annulus by differential quadrature method. Journal of Heat and Mass Transfer 2002;38:597-608.

[17] Shu C, Wu YL. Domain-free discretization method for doubly connected domain and its application to simulate natural convection in eccentric annuli. Computer Methods in Applied Mechanics and Engineering 2002;191(17-18):1827-1841.

[18] Moukalled F, Acharya S. Natural convection in the annulus between concentric horizontal circular and square cylinders. Journal of Thermophysics and Heat Transfer 1996;10(3):524-531.

[19] de Vahl Davis G. Natural convection of air in a square cavity: a benchmark numerical solution. International Journal for Numerical Methods in Fluids 1983;3:249-264.

[20] Kuehn TH, Goldstein RJ. An experimental and theoretical study of natural convection in the annulus between horizontal concentric cylinders. Journal of Fluid Mechanics. 1976;74(4):695-719.

[21] Manzari MT. An explicit finite element algorithm for convection heat transfer problems. International Journal of Numerical Methods for Heat & Fluid Flow 1999;9(8):860-877.

[22] Sammouda H, Belghith A, Surry C. Finite element simulation of transient natural convection of low-Prandtl-number fluids in heated cavity. International Journal of Numerical Methods for Heat & Fluid Flow 1999;9(5):612-624.

[23] Glakpe EK, Watkins CB, Cannon JN. Constant heat flux solutions for natural convection between concentric and eccentric horizontal cylinders. Numerical Heat Transfer, Part B: Fundamentals 1986;10:279-295.

[24] Kaminski DA, Prakash C. Conjugate natural convection in a square enclosure: effect of conduction in one of the vertical walls. International Journal of Heat and Mass Transfer 1986;29(12):1979-1988.

[25] Hribersek M, Skerget L. Fast boundary-domain integral algorithm for the computation of incompressible fluid flow problems. International Journal for Numerical Methods in Fluids 1999;31:891-907.

[26] Kitagawa K, Wrobel LC, Brebbia CA, Tanaka M. A boundary element formulation for natural convection problems. International Journal for Numerical Methods in Fluids 1988;8:139-149.

[27] Le Quere P. Accurate solutions to the square thermally driven cavity at high Rayleigh number. Computers and Fluids 1991;20(1):29-41.

[28] Shu C. Application of differential quadrature method to simulate natural convection in a concentric annulus. International Journal for Numerical Methods in Fluids 1999;30:977-993.

[29] Ding H, Shu C, Yeo, KS, Lu ZL. Simulation of natural convection in eccentric annuli between a square outer cylinder and a circular inner cylinder using local MQ-DQ method. Numerical Heat Transfer, Part A: Applications 2005;47(3):291-313.

Re	1	100	500	1000
L		0.55		
		ψ_w		
Present method	0.0581	0.0582	0.0586	0.0596
FDM [15]	0.0625	0.0626	0.0621	0.0600
L		1		
		ψ_w		
Present method	0.4622	0.4617	0.4500	0.4264
FDM [15]	0.4656	0.4577	0.4465	0.4375

Table 1: Example 1 (rotating cylinder): Comparison of the stream-function values at the inner cylinder, ψ_w, for Re from 1 to 1000 between the present technique (grid of 52×52) and finite difference technique.

Grid	k_{eqo} (outer cylinder)	k_{eqi} (inner cylinder,)
41×41	3.465	3.254
51×51	3.241	3.187
61×61	3.167	3.174
FDM [20]	3.226	3.308
DQM [16]	3.179	3.187

Table 2: Example 2 (symmetric flow, circular-circular annulus): Convergence study of the computed average equivalent conductivities with grid refinement for $Ra = 7 \times 10^4$.

ε	0.25	0.5	0.75	0.95
φ		-90^0		
		ψ_{max}		
Present method	22.19	20.72	18.50	15.71
DQM [16]	22.16	20.62	18.32	15.50
φ		90^0		
		ψ_{max}		
Present method	11.26	9.64	8.25	7.28
DQM [16]	11.13	9.55	8.12	7.17

Table 3: Example 2 (symmetric flow, eccentric circular-circular annuli): Comparison of the maximum stream-function values, ψ_{max}, for two special cases $\varphi = \{-90^0, 90^0\}$ between the present technique and DQM technique.

ε	0.25	0.5	0.75	0.95
φ		45^0		
		ψ_w		
Present method	0.52	1.25	1.01	0.01
DQM [16]	0.52	1.31	1.07	0.03
DFD [17]	0.54	1.29	1.09	0.03
φ		0^0		
		ψ_w		
Present method	0.60	1.28	1.18	0.01
DQM [16]	0.72	1.15	1.30	0.06
DFD [17]	0.72	1.10	1.26	0.06
φ		-45^0		
		ψ_w		
Present method	0.48	0.80	1.05	0.6
DQM [16]	0.51	0.92	0.99	0.08
DFD [17]	0.51	0.77	0.77	0.04

Table 4: Example 2 (unsymmetrical flow, eccentric circular-circular annuli): Comparison of the stream-function values at the inner cylinders, ψ_w, for $\varepsilon = \{0.25, 0.5, 0.75, 0.95\}$ and $\varphi = \{-45^0, 0^0, 45^0\}$ between the present, DQM and DFD techniques.

ε	0.25	0.5	0.75	0.95
φ		45^0		
		ψ_{max}		
Present method	15.31	14.23	13.52	12.91
MQ-DQ [29]	15.32	14.35	13.61	12.98
φ		0^0		
		ψ_{max}		
Present method	17.00	16.99	16.87	17.18
MQ-DQ [29]	17.00	16.97	16.84	
φ		-45^0		
		ψ_{max}		
Present method	18.50	20.09	21.02	21.61
MQ-DQ [29]	18.50	20.03	21.01	21.68

Table 5: Example 3 (eccentric square-circular annuli): Comparison of the maximum stream-function values, ψ_{max}, for $\varepsilon = \{0.25, 0.5, 0.75, 0.95\}$ and $\varphi = \{-45^0, 0^0, 45^0\}$ between the present technique and MQ-DQ technique.

ε	0.25	0.5	0.75	0.95
φ		-90^0		
		ψ_{max}		
Present method	18.63	21.30	23.47	24.48
MQ-DQ [29]	18.64	21.29	23.52	
φ		90^0		
		ψ_{max}		
Present method	12.37	11.36	10.10	9.289
MQ-DQ [29]	12.39	11.38	10.09	

Table 6: Example 3 (eccentric square-circular annuli): Comparison of the maximum stream-function values, ψ_{max}, for special cases $\varphi = \{-90^0, 90^0\}$ between the present technique and MQ-DQ technique.

Ra	10^4	5×10^4	10^5	5×10^5	10^6
			Nu_o		
Present method	3.22	4.04	4.89	7.43	8.70
MQ-DQ [29]	3.24		4.86		8.90
FDM [18]	3.33		5.08		9.37
			Nu_i		
Present method	3.21	4.04	4.89	7.51	8.85
MQ-DQ [29]	3.24		4.86		8.90
FDM [18]	3.33		5.08		9.37

Table 7: Example 3 (square-circular annulus): Comparison of the average Nusselt number on the outer and inner cylinders, Nu_o and Nu_i, for Ra from 10^4 to 10^6 between the present technique (grid of 62×62) and some other techniques.

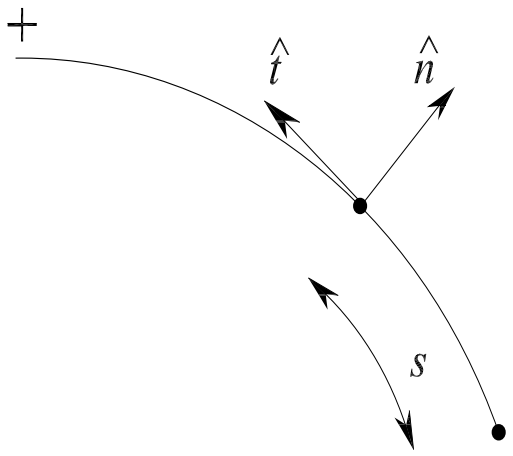

Figure 1: A curved boundary.

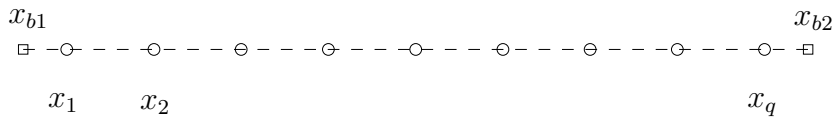

Figure 2: Points on a grid line consist of interior points x_i ($\circ$) and boundary points x_{bi} ($\square$).

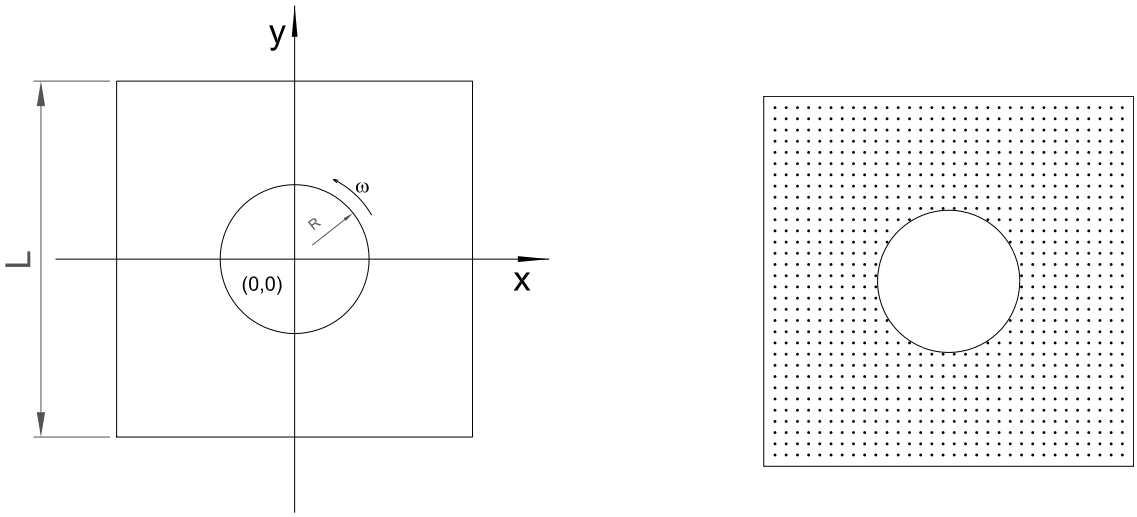

Figure 3: Example 1 (rotating cylinder): geometry and discretisation.

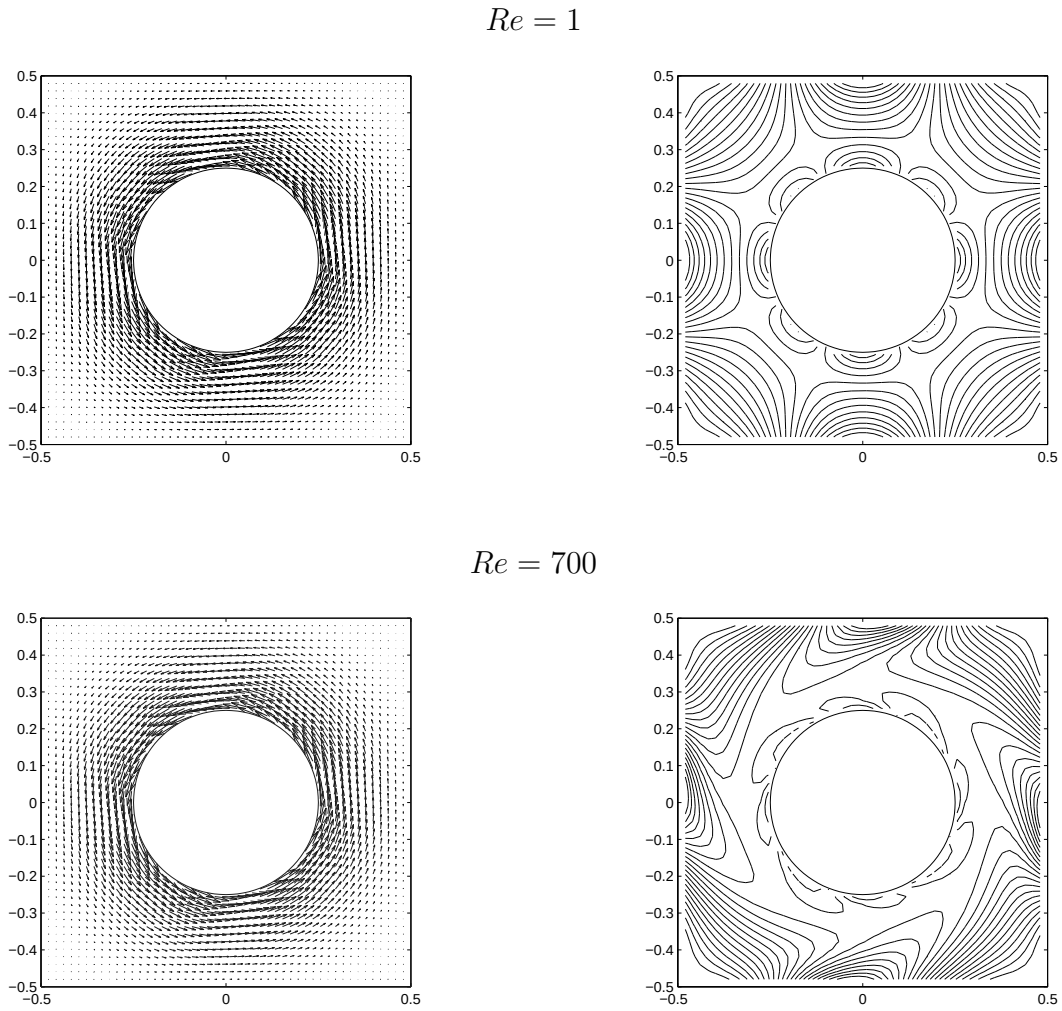

Figure 4: Example 1 (rotating cylinder): Velocity field (left) and vorticity field (right) for the flow at $Re = 1$ and $Re = 700$.

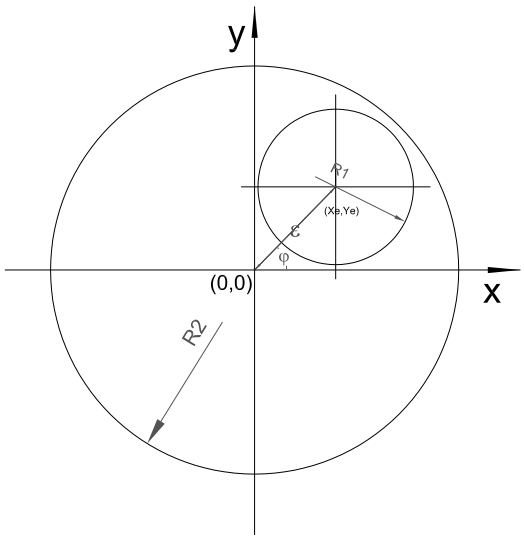

Figure 5: Example 2 (eccentric circular-circular annulus): geometry.

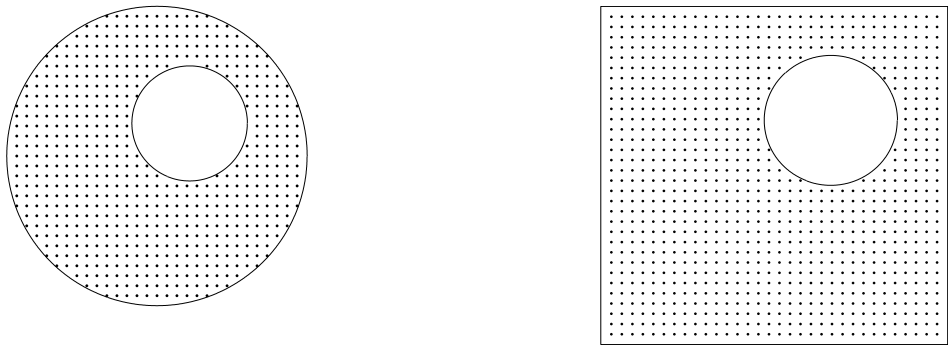

(a) (b)

Figure 6: Schematic spatial discretisations for annulus between two circular cylinders (a) and annulus between inner circular and outer square cylinders (b).

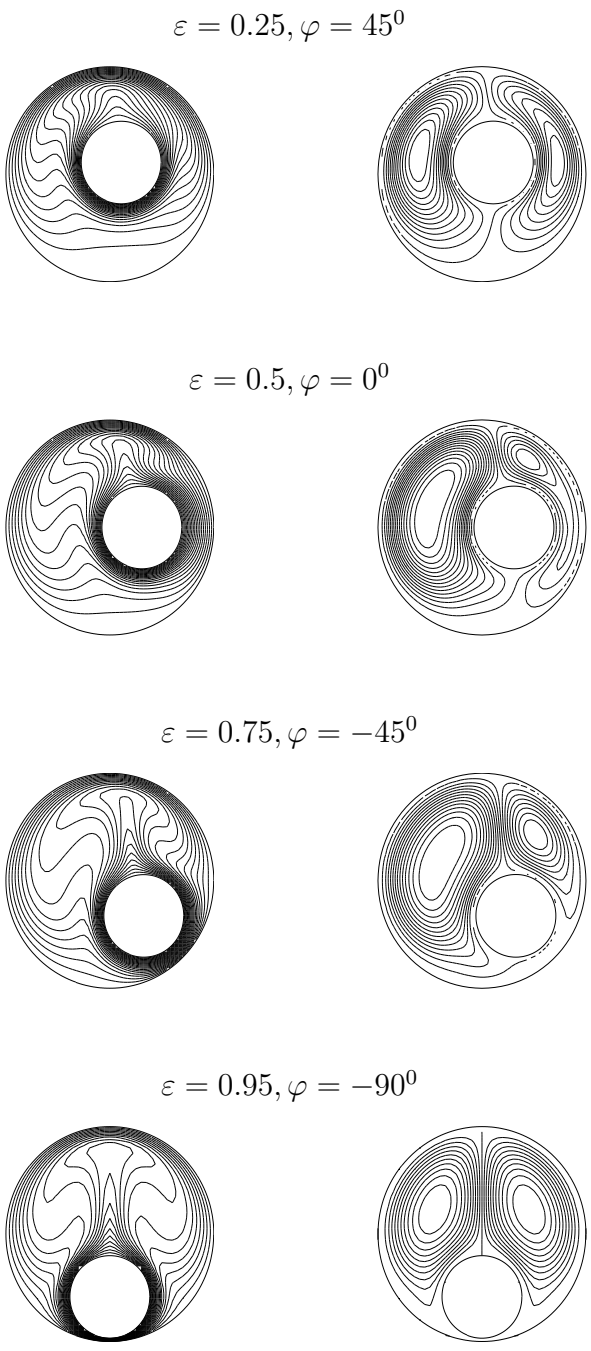

Figure 7: Example 2 (circular-circular annulus): Contour plots for the temperature (left) and stream-function (right) fields with respect different values of eccentricity ε and angular directions φ for the flow at $Ra = 1 \times 10^4$. Each plot contains 21 contour lines whose levels vary linearly from the minimum to maximum values.

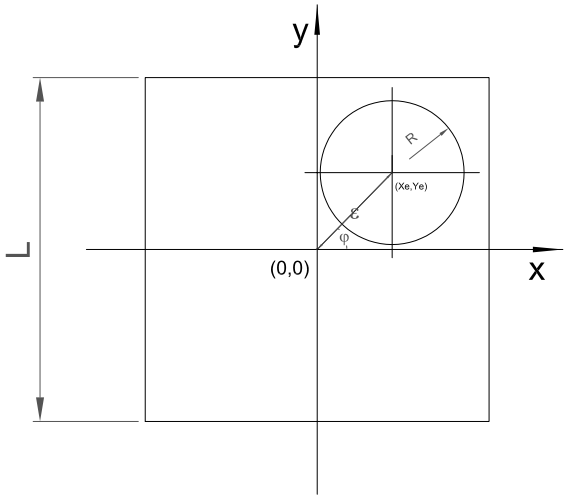

Figure 8: Example 3 (eccentric square-circular domain): geometry.

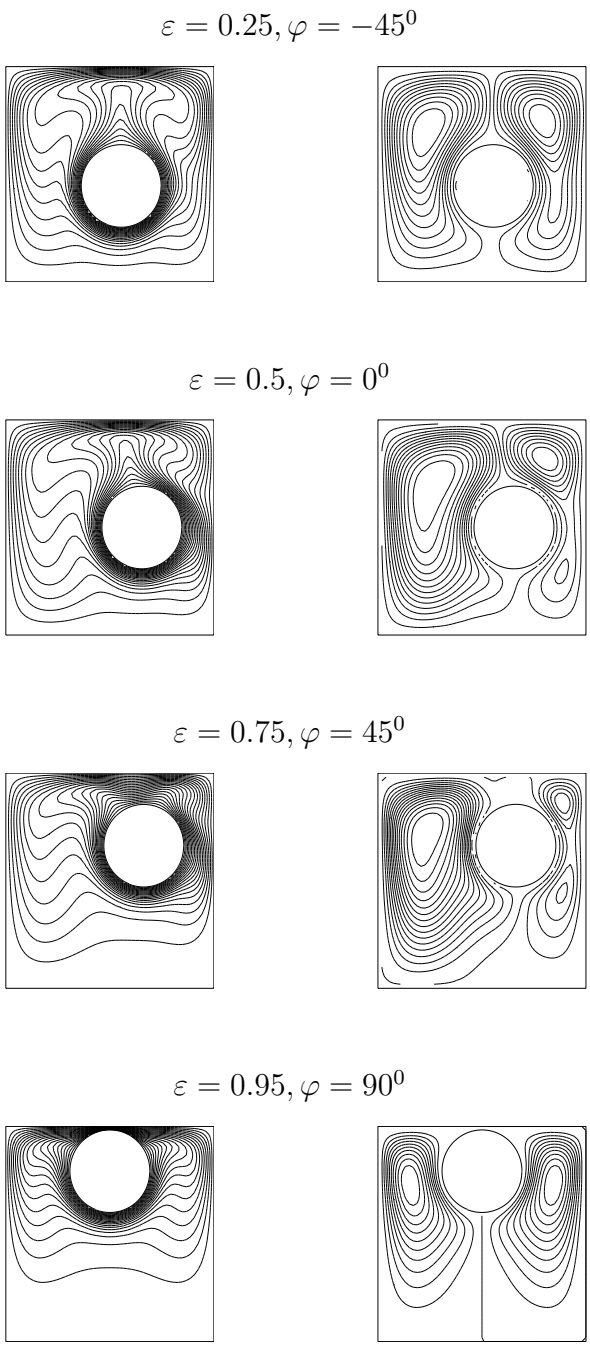

Figure 9: Example 3 (square-circular annulus): The temperature (left) and stream-function (right) fields with respect different values of eccentricity ε and angular direction φ for the flow at $Ra = 3 \times 10^5$. Each plot contains 21 contour lines whose levels vary linearly from the minimum to maximum values.

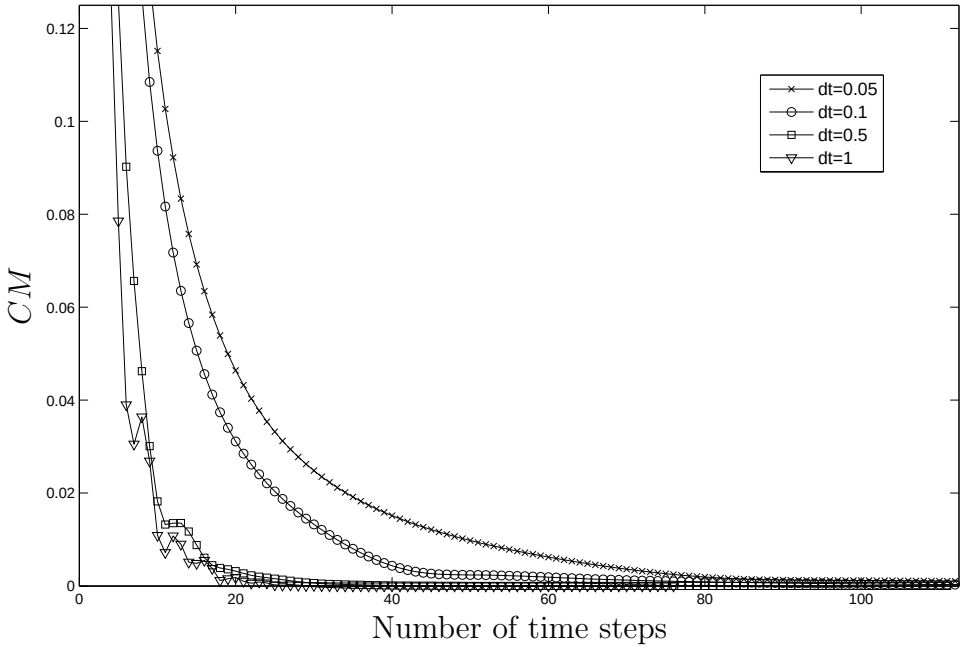

Figure 10: Example 3 (eccentric square-circular domain): the effects of time-step length on the convergence.